



Graphite|LiFePO₄ lithium-ion battery working at the heat engine coolant temperature



Andrzej Lewandowski, Beata Kurc*, Agnieszka Swiderska-Mocek, Natalia Kusa

Faculty of Chemical Technology, Poznan University of Technology, PL-60 965 Poznan, Poland

HIGHLIGHTS

- Possibility of Li-ion cell operation in the cooling system of a car heat engine (90 °C) was demonstrated.
- Electrodes were characterized by EIS, SEM and charging/discharging tests.
- Impedance of the system decreased with increased temperature.
- The system showed high capacity at increased temperature.
- The electrolyte was characterized by low vapor pressure and decreased ignition point.

ARTICLE INFO

Article history:

Received 30 December 2013

Received in revised form

11 April 2014

Accepted 17 April 2014

Available online 10 May 2014

Keywords:

LiFePO₄ cathode

Sulpholane

In the cooling system of a car heat engine (90 °C)

Li-ion battery

ABSTRACT

Electrochemical properties of the graphite anode and the LiFePO₄ cathode, working together with the 1 M LiPF₆ in TMS (sulpholane) at 90 °C have been studied. The general aim of the investigation was to demonstrate a potential application for a Li-ion cell working in the cooling system of a car heat engine (90 °C). Electrodes were characterized with the use of electrochemical impedance spectroscopy (EIS), scanning electron microscopy (SEM) as well as galvanostatic charging/discharging tests. SEM images of both electrodes after charging/discharging processes were covered with a film (electrochemical SEI formation). The charge transfer resistance at 90 °C, R_{ct} , of the C₆Li|Li⁺ anode and the LiFePO₄ cathode was 24 Ω and 110 Ω, respectively. Reversible capacity of the LiC₆ anode after 10–20 cycles, at a low current rate was close to the theoretical value of 370 mAh g^{−1} however an increasing current rate decreased to ca. 200 mAh g^{−1} (for 1C). The reversibility of the process was close to 95%. The capacity of the LiFePO₄ cathode was ca. 150 mAh g^{−1}, almost independent of the current rate and close to the theoretical value of 170 mAh g^{−1}.

© 2014 Elsevier B.V. All rights reserved.

1. Introduction

The market of hybrid vehicles (HV), powered by both heat and electric engines, has been currently developing rapidly. Temperature control of the battery stack is important from the point of view of its efficiency, lifetime and safety. However, the operation of Li-ion batteries at a relatively high temperature may cause an increased pressure (electrolyte solvent vapor) as well as a unit cell mechanical damage, while a low temperature suppresses the rate of faradaic reactions leading to reduced power output [1]. Batteries temperature is controlled by their separate cooling system. A

common battery pack configuration is a stack of rectangular or spherical battery cells; with temperature control provided by a cooling fluid. Thermal management of lithium-ion batteries and their stacks have been analyzed [1–8], including the graphite|LiFePO₄ system [9,10]. As a result, a hybrid vehicle contains two separate cooling systems working at different coolant temperatures, serving the heat engine and battery stack. The general aim of this study was to verify the concept of thermal control of the battery stack with the heat engine cooling system, which would result in simplification of HV construction. However, such a concept cannot be practically carried out with the use of commercial Li-ion batteries filled with electrolytes containing LiPF₆ salt dissolved in cyclic carbonates, characterized by a relatively high vapor pressure (temperature of vehicle heat engine coolant is ca. 90 °C). In order to decrease the electrolyte pressure inside the unit cell, a solvent-free

* Corresponding author.

E-mail address: beata.kurc@put.poznan.pl (B. Kurc).

ionic liquid [11] or low vapor pressure solvent should be used as a component of the electrolyte.

It has been demonstrated recently that an electrolyte based on lithium salt dissolved in sulfolane (tetramethylene sulphone, TMS) may be used in the graphite|LiFePO₄ cell [12]. The TMS is characterized by a high boiling point ($T_b = 280\text{ }^\circ\text{C}$) and a low vapor pressure [13]. For this reason, in the present paper performance of the graphite|LiFePO₄ cell, working together with the TMS based electrolyte, was investigated at the temperature of the engine coolant ($90\text{ }^\circ\text{C}$).

2. Experimental

2.1. Materials

Graphite (G, SL-20, BET surface area $6.0\text{ m}^2\text{ g}^{-1}$, Superior Graphite, USA), carbon black (CB, Fluka), poly(vinylidene fluoride) (PVdF, $M_w = 180\,000$ Fluka), lithium foil (Aldrich, 0.75 mm thick), vinylene carbonate (VC, Aldrich), *N*-methyl-2-pyrrolidinone (NMP, Fluka), lithium hexafluorophosphate (LiPF₆, Aldrich), sulfolane (TMS, Fluka) and lithium iron phosphate (LiFePO₄, carbon coated, battery grade, BET surface area $15.4\text{ m}^2\text{ g}^{-1}$, Aldrich) were used as received.

Electrolytes were obtained by dissolution of the LiPF₆ solid salt in liquid TMS heated to ca. $35\text{ }^\circ\text{C}$ (TMS is solid at room temperature). Electrolytes contained VC as the SEI forming additive (10%). Tested anodes were prepared on a copper foil (Hohsen, Japan) by a casting technique, from a slurry of graphite, carbon black and PVdF in NMP. The ratio of components was G:CB:PVdF = 85:5:10 (by weight). After solvent (NMP) evaporation at $120\text{ }^\circ\text{C}$ in a vacuum, a layer of the carbon electrode containing an active material (G), an electronic conductor (CB) and the binder (PVdF) was formed. The tested LiFePO₄ cathode was prepared by casting LiFePO₄ + G + PVdF (ratio 85:10:5) slurry in *N*-methyl-2-pyrrolidinone (NMP, Fluka) on the aluminum current collector (diameter 12 mm) (NMP evaporated in vacuum at $120\text{ }^\circ\text{C}$).

2.2. Procedures and measurements

Electrochemical properties of the cells were characterized by using electrochemical impedance spectroscopy (EIS) and galvanostatic charging/discharging tests. The cycling measurements were taken with the use of the ATLAS 0461 MBI multichannel electrochemical system (Atlas-Sollich, Poland) at different current rates (C/5–1C). Charging/discharging measurements were carried out at $90\text{ }^\circ\text{C}$. Cyclic voltammetry (CV) and ac impedance measurements

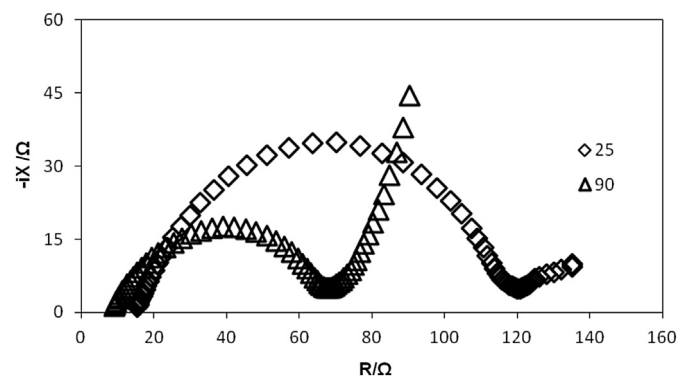


Fig. 1. Impedance spectra of the C₆Li|Li system as a function of temperature. The lithiated graphite electrode (C₆Li) was after three working cycles (intercalation deintercalation/intercalation). Graphite mass: 3.49 mg.

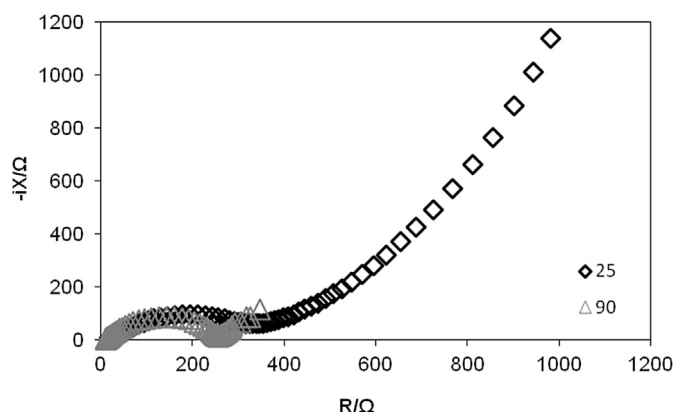


Fig. 2. Impedance spectra of the LiFePO₄|Li system as a function of temperature. The cathode was after three working cycles (intercalation deintercalation/intercalation). LiFePO₄ mass: 2.80 mg.

were performed using the μ Autolab FRA2 type III electrochemical system (Ecochemie, Netherlands).

Electrodes were separated by the glass microfiber GF/A separator (Whatmann, 0.4 mm–0.6 mm thick), placed in an adopted Swagelok® connecting tube. Typically, the mass of the electrodes was as follows: Li: ca. 45 mg (0.785 cm^2), graphite: 3.5–4.0 mg, LiFePO₄: 2.0–3.0 mg. Cell assembling was performed in a glove box in the dry argon atmosphere.

After electrochemical measurements the cells were disassembled, graphite electrodes were washed with DMC and dried in the vacuum at room temperature. The morphology of electrodes and polymer electrolytes was observed with a scanning electron microscopy (SEM, Tescan Vega 5153). All operations were made in a dry argon atmosphere in a glove box.

3. Results and discussion

3.1. Impedance studies

3.1.1. Electrolyte resistance

Figs. 1 and 2 present impedance spectra of C₆Li|electrolyte|Li and LiFePO₄|electrolyte|Li cells. Spectra were deconvoluted according to the equivalent circuit shown in Fig. 3. The conductivity of 1.0 M LiPF₆ in TMS at $25\text{ }^\circ\text{C}$ was 2.6 mS cm^{-1} , with the activation energy of the conduction process $E_a = 18.4\text{ kJ mol}^{-1}$ [14]. Therefore, the specific conductivity of the electrolyte at $90\text{ }^\circ\text{C}$ was 9.8 mS cm^{-1} , which is comparable to the corresponding value characteristic of classical solutions in cyclic carbonates working at room temperature [15].

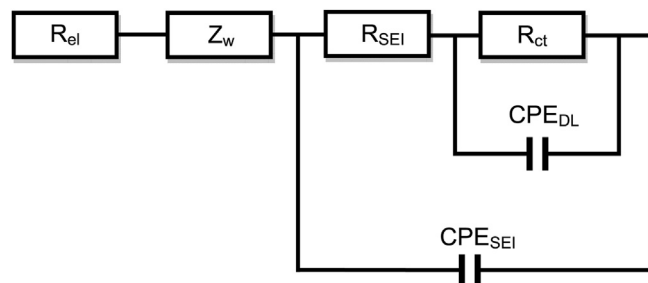


Fig. 3. Equivalent circuit used for impedance spectra deconvolution of the LiFePO₄|SEI|Li⁺ and LiC₆|SEI|Li⁺ systems.

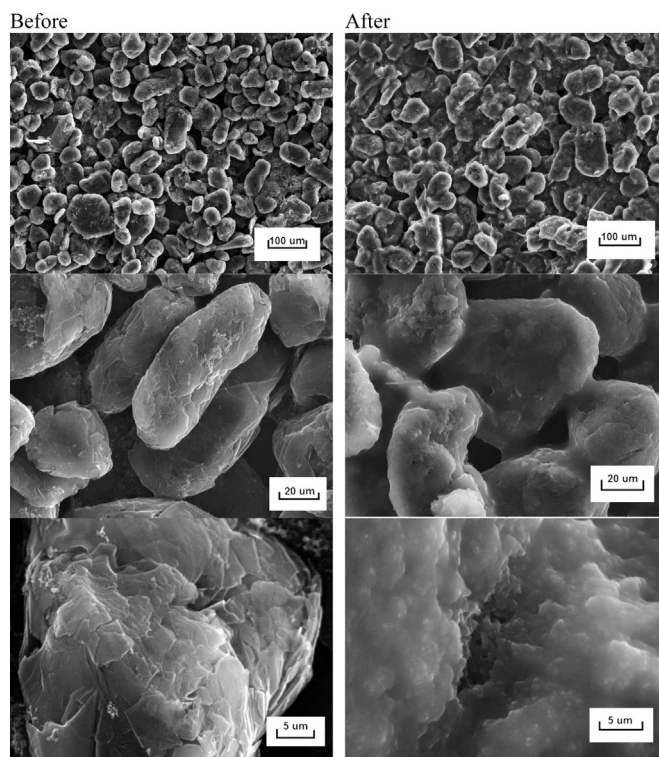


Fig. 4. SEM images of the graphite electrode before and after charging/discharging (100 cycles). $T = 90\text{ }^{\circ}\text{C}$.

Corresponding resistance of the electrolyte in cells, R_{el} , was somewhat higher than that expected from its conductance, due to the porous structure of both electrodes. However, at $90\text{ }^{\circ}\text{C}$ it decreased considerably to ca. $8\text{ }\Omega$.

3.1.2. SEI resistance

The resistance of the SEI layer, R_{SEI} , formed at $25\text{ }^{\circ}\text{C}$ on the graphite anode and the LiFePO_4 cathode was ca. $9\text{ }\Omega$ and $51\text{ }\Omega$, respectively. The corresponding value for SEI formed at $90\text{ }^{\circ}\text{C}$, was

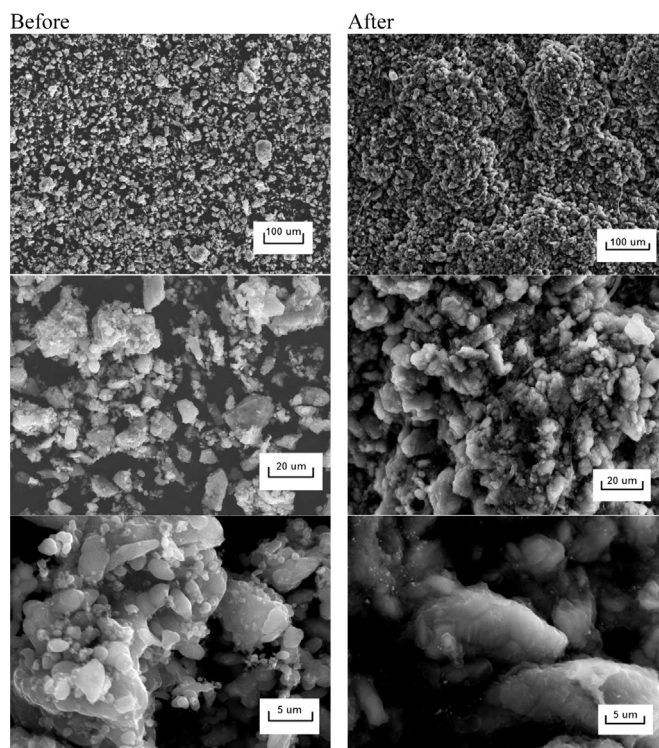


Fig. 5. SEM images of the LiFePO_4 electrode before and after charging/discharging (100 cycles). $T = 90\text{ }^{\circ}\text{C}$.

higher, achieving 32 Ω (C_6Li) and 67 Ω ($LiFePO_4$). A possible explanation is that at a higher temperature the thickness of the formed SEI layer was higher. SEM images of both electrodes before and after the charging/discharging process (electrochemical SEI formation) are shown in Figs. 4 and 5. In both cases the electrodes after electrochemical cycling were covered with a film. Small particles of the $LiFePO_4$ material were agglomerated and covered with SEI after charging/discharging.

3.1.3. Charge transfer resistance

Charge transfer resistance, R_{ct} , of the $C_6Li|Li^+$ anode was ca. 93 Ω at 25 $^{\circ}C$ to decrease to ca. 24 Ω at 90 $^{\circ}C$. The corresponding R_{ct} value for the $LiFePO_4$ cathode is much higher: ca. 260 Ω at 25 $^{\circ}C$ and ca. 110 Ω at 90 $^{\circ}C$.

Charge transfer resistance may be converted into the surface area independent exchange current density:

$$j_0 = \frac{RT}{FA} \frac{1}{R_{ct}} \quad (1)$$

where A is the electrode material real surface area, while the other symbols have their usual meaning.

In the case of the graphite/ Li^+ system, the real surface area was ca. 209 cm^2 (ca. 3.49 mg, BET specific area 6.0 $m^2 g^{-1}$). This leads to

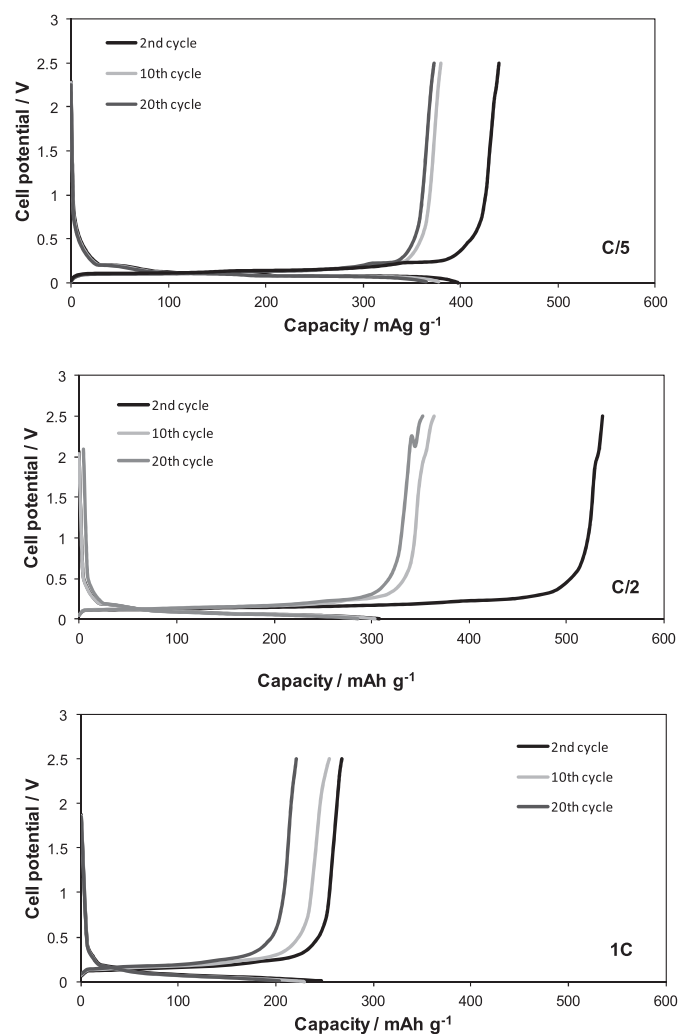


Fig. 6. Galvanostatic charging/discharging profiles of the $C_6Li|Li$ cell at different current rates (C/5, C/2 and 1C). $T = 90^{\circ}C$.

the exchange current density of ca. $1.23 \times 10^{-4} A cm^{-2}$ and $1.50 \times 10^{-4} A cm^{-2}$ at 25 $^{\circ}C$ and 90 $^{\circ}C$, respectively.

The corresponding charge transfer resistance for the $LiFePO_4|Li^+$ cathode (ca. 2.80 mg, BET specific area 15.4 $m^2 g^{-1}$, real surface area $A = 431 cm^2$) was lower: ca. $5.96 \times 10^{-5} A cm^{-2}$ and $7.26 \times 10^{-5} A cm^{-2}$ at 25 $^{\circ}C$ and 90 $^{\circ}C$, respectively.

3.1.4. Diffusion impedance

The line at the low-frequency region is due to the diffusion of the electro-active species. Generally, any software system used for EIS curve deconvolution applies the Warburg model, which is based on a symmetrical constant phase element. Hence, the diffusion process was approximated here also by the Warburg element Z_W . Slopes of linear parts of impedance spectra were not exactly 45 $^{\circ}$, as predicted by the Warburg model. Moreover, in the case of the $C_6Li|Li^+$ anode, the diffusion impedance increases with an increasing temperature, which is difficult to explain. However, the $LiFePO_4$ cathode diffusion impedance decreases considerably with the temperature increase. Numerical evaluation of the diffusion coefficient of Li in the graphite anode or the $LiFePO_4$ cathode is impossible as the concentrations of diffusing species in the solid state have been unknown.

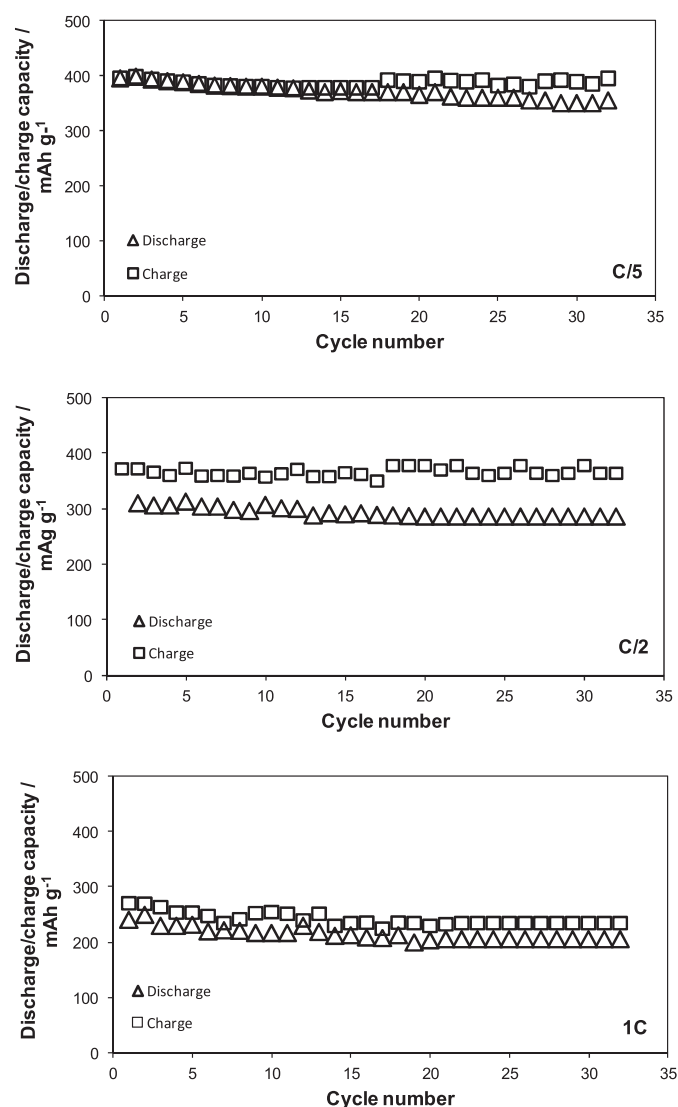


Fig. 7. Charge and discharge capacity of the graphite (C_6Li) electrode at different current rates (C/5, C/2 and 1C). $T = 90^{\circ}C$.

3.2. Charging/discharging

Charging and discharging profiles for the C_6Li anode (2-nd, 10-th and 20-th cycle), for different current rates (C/5, C/2 and 1C) are shown in Fig. 6. Reversible capacity after 10, 20 cycles, at the lowest current rate (C/5) was close to the theoretical value of 370 mAh g^{-1} while its irreversible initial value was ca. 400 mAh g^{-1} . However, with an increasing current rate the reversible discharge capacity decreased to ca. 200 mAh g^{-1} for 1C. The reversibility of the process was close to 95% (Fig. 7). The corresponding charging/discharging curves for the $LiFePO_4$ cathode can be seen in Fig. 8. The capacity of ca. 150 mAh g^{-1} was almost independent of the current rate and close to the theoretical value of ca. 170 mAh g^{-1} . However, the coulombic efficiency is ca. 75% (Fig. 9). The reversibility of the process was close to 95% at the C/5. The capacity of the $LiFePO_4$ cathode was ca. 150 mAh g^{-1} , almost independent of the current rate and close to the theoretical value of ca. 170 mAh g^{-1} . Performance of about 75% was achieved at the 1C rate.

Moreover, a long cyclic life for the $LiFePO_4$ cathodes of 1500–2400 cycles have been achieved in laboratory tests [16–20]. However, the challenge is to develop an adequate testing protocol that can effectively simulate and predict the battery performance in EV services [6]. The possible mechanisms of capacity degradation of the $LiFePO_4$ cathode include: (1) loss of Li through side reactions; (2) loss of active material due to cracking and dissolution; (3) the

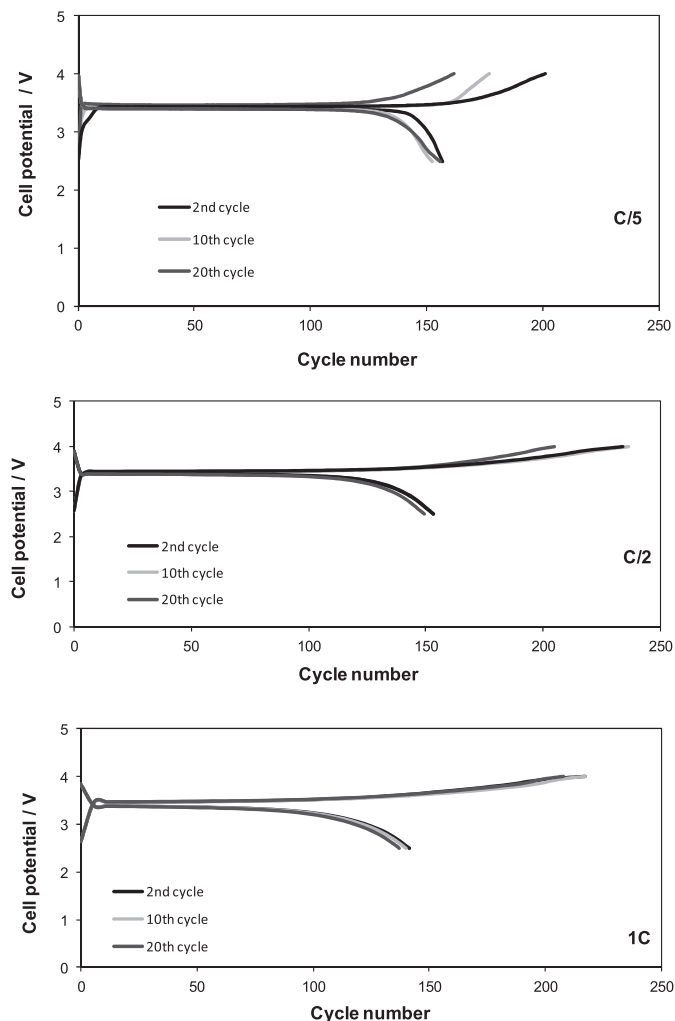


Fig. 8. Galvanostatic charging/discharging profiles of the $LiFePO_4/Li$ cell at different current rates (C/5, C/2 and 1C). $T = 90^\circ\text{C}$.

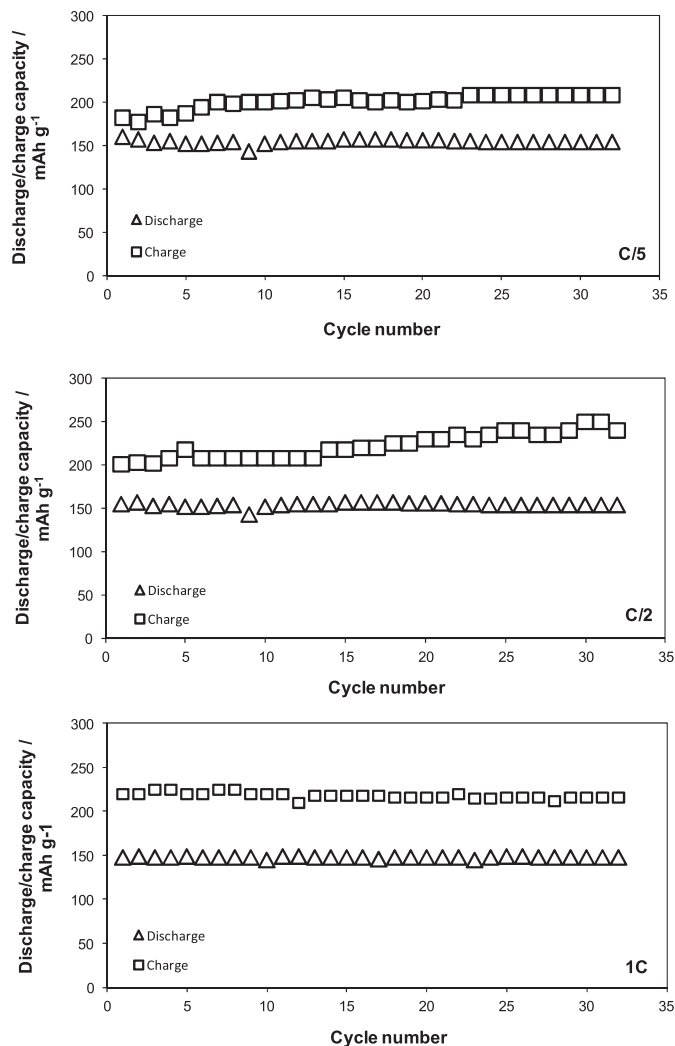


Fig. 9. Charge and discharge capacity of the $LiFePO_4$ electrode at different current rates (C/5, C/2 and 1C). $T = 90^\circ\text{C}$.

rise of cell impedance due to changes of the SEI layer (surface–electrolyte-interface) and (4) physical degradation of electrode structure [21–26]. Among these, effects due to SEI formation is considered to be the major cause [27]. At high temperatures, the specific capacity of the $LiFePO_4$ cathode was reported to be improved due to the increased lithium diffusion rate and electron transfer activity [28,29]. However, there is a literature report that the cycling or storing capacity of the $LiFePO_4$ material decreased with increasing temperature [30]. The cause of capacity fade at elevated temperature has been attributed to the increased dissolution of Fe-ions from $LiFePO_4$ particles into the electrolyte, which are then deposited on the graphite anode surface. The deposited Fe catalyzes the formation of SEI films, leading to an increase of interfacial impedance of graphite electrodes [30]. The high temperature stability was improved with a LiBOB electrolyte or $Li_4Ti_5O_{12}$ anode [23,31].

Fig. 10 shows the dependence of capacitance of the $LiFePO_4/1 \text{ M LiPF}_6$ in TMS + 10% wt. VC/G on the number of cycles. The charging capacity of the $LiFePO_4/G$ cell was ca. 270 mAh g^{-1} after the first cycle to stabilize at about 240 mAh g^{-1} after 100 cycles. The $LiFePO_4/1 \text{ M LiPF}_6$ in TMS + 10% wt. VC/G system showed higher capacity (after 100 cycles) at 90°C in comparison to the room temperature operation. When cycled at 25°C the cell lost 0.02% of its capacity per cycle. At 90°C the capacity fading rate is decreased.

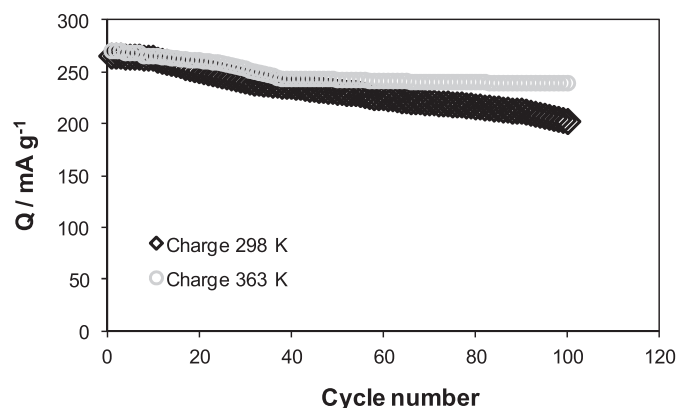


Fig. 10. Charge capacity of the LiFePO_4 /1 M LiPF_6 in TMS + 10% wt. VC/G. Current rate C/5.

In comparison in the literature [32] we could find different results. The linear relationship between capacity retention and cycle number implies that a single factor dominating the capacity degradation of the cell during the long-term cycles. As expected, long-term cycling behavior of the cell is strongly affected by temperature. At elevated temperatures, the cycle life of the cell was greatly shortened. The cell underwent 544 cycles at 25 °C whereas it lasted only 247 cycles at 60 °C. The average capacity fading rates at different temperatures shows the influence of temperature on the capacity-fading rate. When cycled at 25 °C, the cell lost 0.048% of its capacity per cycle. At 60 °C, the capacity fading rate is increased to 0.121%, which is about 2.3 times as high as that cycled at 25 °C [32].

4. Conclusions

The specific conductivity of the electrolyte at 90 °C is ca. 9.8 mS cm^{-1} , which is comparable to the corresponding value characteristic of classical solutions in cyclic carbonates working at room temperature. SEM images of both electrodes after the charging/discharging process were covered with a film (electrochemical SEI formation). Charge transfer resistance at 90 °C, R_{ct} , of the $\text{C}_6\text{Li}|\text{Li}^+$ anode and the LiFePO_4 cathode was ca. 24Ω and 110Ω , respectively.

Reversible capacity of the LiC_6 anode after 10, 20 cycles at a low current rate was close to the theoretical value of 370 mAh g^{-1}

while with an increasing current rate it decreased to ca. 200 mAh g^{-1} (for 1C).

Acknowledgments

Support of grant 31-277/2014 DSPB is gratefully acknowledged.

References

- [1] A. Jarret, H.-Y. Kim, J. Power Sources 245 (2014) 644.
- [2] K. Onda, T. Ohshima, M. Nakayama, K. Fukuda, T. Araki, J. Power Sources 158 (2006) 535.
- [3] R.E. Williford, V.V. Viswanathan, Ji-G. Zhang, J. Power Sources 189 (2009) 101.
- [4] V.V. Viswanathan, D. Choi, D. Wang, W. Xu, S. Towne, R.E. Williford, Ji-G. Zhang, J. Liu, Z. Yang, J. Power Sources 195 (2010) 3720.
- [5] Ji Xun, R. Liu, K. Jiao, J. Power Sources 233 (2013) 47.
- [6] X. Li, F. He, L. Ma, J. Power Sources 238 (2013) 395.
- [7] M. Xiao, S.-Y. Choe, J. Power Sources 241 (2013) 46.
- [8] H. Fathabadi, J. Power Sources 245 (2014) 495.
- [9] C. Forgez, D.V. Do, G. Friedrich, M. Morcrette, C. Delacourt, J. Power Sources 195 (2010) 2961.
- [10] K. Jalkanen, T. Aho, K. Vuorilehto, J. Power Sources 243 (2013) 354.
- [11] A. Lewandowski, A. Swiderska-Mocek, J. Power Sources 194 (2009) 601.
- [12] A. Lewandowski, B. Kurc, I. Stepniak, A. Swiderska-Mocek, Electrochim. Acta 56 (2011) 5972.
- [13] J. Martinmaa, in: J.J. Lagowski (Ed.), Sulfolane in the Chemistry of Nonaqueous Solvents, vol. IV, Academic Press, 1976.
- [14] V.S. Kolosnitsyn, L.V. Sheina, S.E. Mochalov, Russ. J. Electrochem. 44 (2008) 575.
- [15] M. Morita, M. Ishikawa, Y. Matsuda, in: M. Wakihara, O. Yamamoto (Eds.), Lithium Ion Batteries, Wiley, 1998.
- [16] J. Liu, J. Wang, X. Yan, X. Zhang, G. Yang, A.F. Jalbout, R. Wang, Electrochim. Acta 54 (2009) 5656.
- [17] M.E. Zhong, Z.T. Zhou, Mater. Chem. Phys. 119 (2010) 428.
- [18] Y.J. Gu, C.S. Zeng, H.K. Wu, H.Z. Cui, X.W. Huang, X.B. Liu, C.L. Wang, Z.N. Yang, H. Liu, Mater. Lett. 61 (2007) 4700.
- [19] S.B. Peterson, J. Apt, J.F. Whiteacre, J. Power Sources 195 (2010) 2385.
- [20] X. Yan, G. Yang, J. Liu, Y. Ge, H. Xie, X. Pan, R. Wang, Electrochim. Acta 54 (2009) 5770.
- [21] M. Dubarry, V. Svoboda, R. Hwu, B.Y. Liaw, J. Power Sources 174 (2007) 366.
- [22] J. Shim, K.A. Striebel, J. Power Sources 119 (2003) 955.
- [23] K. Amine, J. Liu, I. Belharouak, Electrochem. Commun. 7 (2005) 669.
- [24] K. Striebel, J. Shim, A. Sierra, H. Yang, X. Song, R. Kostecki, K. McCarthy, J. Power Sources 146 (2005) 33.
- [25] D. Wang, X. Wu, Z. Wang, L. Chen, J. Power Sources 140 (2005) 125.
- [26] H.H. Chang, H.C. Wu, N.L. Wu, Electrochem. Commun. 10 (2008) 1823.
- [27] Q. Zhang, R.E. White, J. Power Sources 173 (2007) 990.
- [28] M. Dubarry, B.Y. Liaw, J. Power Sources 194 (2009) 541.
- [29] M. Takahashi, S. Tobishima, K. Takei, Y. Sakurai, Solid State Ionics 148 (2002) 283.
- [30] S.H. Wu, K.M. Hsiao, W.R. Liu, J. Power Sources 146 (2005) 550.
- [31] F. Mestre-Aizpurua, S. Hamelet, C. Masquelier, M.R. Palacin, J. Power Sources 195 (2010) 6897.
- [32] T.L. Zhanga, Q. Suna, M. Shenb, Q. Qua, H. Zhenga, Electrochim. Acta 111 (2013) 802.